Crystal chemistry of FeO at high pressure and temperature

YINGWEI FEI

Center for High Pressure Research and Geophysical Laboratory, Carnegie Institution of Washington,
5251 Broad Branch Road, NW, Washington, DC 20015, U.S.A.

Abstract—The phase relations and equations of state of Fe_xO have been studied up to a pressure of 100 GPa and a temperature of 1100 K, using a high-temperature diamond-anvil cell combined with synchrotron x-ray diffraction. Under a hydrostatic environment, Fe_xO transforms from the NaCl-type cubic structure (B1) to a rhombohedral structure at 16 GPa and 300 K. The transition pressures increase as a function of temperature with a pressure-temperature slope of $0.070(\pm0.003)$ GPa/K. No significant effect of nonstoichiometry on the transition boundary was observed. The transition occurs at lower pressure under nonhydrostatic conditions. The rhombohedral phase increases its distortion with increasing pressure. Further distortions from the rhombohedral cell to a lower symmetry phase were observed at pressures above 40 GPa at room temperature. Upon heating at high pressure, the NiAs-type hexagonal phase (B8) forms at 90 GPa and 600 K. Least-squares fits of the hydrostatic compression data yielded the room-temperature bulk modulus $K_{T0} = 146(\pm2)$ GPa with its pressure derivative $(\partial K_{T0}/\partial P)_T = 4$ for the NaCl-type cubic phase (B1). The effect of degree of nonstoichiometry on the bulk moduli is small, within the uncertainty of the experiments. Although the bulk modulus for the rhombohedral phase cannot be determined accurately, by comparing the structurally related interplanar d spacings it is evident that the rhombohedral phase is less compressible than the cubic phase. The bulk modulus and its pressure derivative for the NiAs-type hexagonal phase (B8), derived from the static compression data, are 172 GPa and 4.3 at 900 K, respectively.

INTRODUCTION

EXPERIMENTAL STUDIES in the system MgO-FeO-SiO$_2$ at high pressure and temperature have provided tight constraints on mantle mineralogy. The crystal chemistry of the end-member FeO at high pressure and temperature is of particular importance in understanding the role of iron in the Earth's lower mantle. Furthermore, FeO has been suggested as a possible light-alloying component in the Earth's core (RINGWOOD, 1977). There has been increasing experimental evidence that high pressure and temperature would enhance the solubility of oxygen in molten iron (KATO and RINGWOOD, 1989; OHTANI and RINGWOOD, 1984; OHTANI *et al.*, 1984; RINGWOOD and HIBBERSON, 1990, 1991; and ITO *et al.*, 1995). In order to understand the fundamental physiochemical basis for those observations, it is essential to determine the crystal and electronic structure transitions and the compression behavior of FeO at high pressure and temperature.

Ferrous oxide is invariably nonstoichiometric with compositions from $Fe_{0.88}O$ to $Fe_{0.98}O$ (HAZEN and JEANLOZ, 1984). Three polymorphs in Fe_xO, the NaCl-type cubic (B1), rhombohedral, and NiAs-type hexagonal (B8) phases, have been identified (ZOU *et al.*, 1980; JEANLOZ and AHRENS, 1980; YAGI *et al.*, 1985; and FEI and MAO, 1994). The rhombohedral and NiAs-type hexagonal phases are not quenchable. The cubic to rhombo-

hedral transition accompanies a magnetic transition from paramagnetic to antiferromagnetic state (TOMBS and ROOKSBY, 1950; WILLIS and ROOKSBY, 1953; ROTH, 1960; VAUGHAN and DRICKAMER, 1967; ZOU *et al.*, 1980). The transition to the NiAs-type hexagonal phase may be associated with the metallization of Fe_xO (KNITTLE and JEANLOZ, 1986, 1991; KNITTLE *et al.*, 1986; and FEI and MAO, 1994). The equation of state for the cubic phase has been studied extensively by static compression method (MAO *et al.*, 1969; WILL *et al.*, 1980; HAZEN, 1981; YAGI *et al.*, 1985; JEANLOZ and SATO-SORENSEN, 1986; LIU and LIU, 1987; and FEI and MAO, 1991) and by ultrasonic and shock-wave experiments (MIZUTANI, 1971; SUMINO *et al.*, 1980; BERGER *et al.*, 1981; BONCZAR and GRAHAM, 1982; JACKSON *et al.*, 1990; and JEANLOZ and AHRENS, 1980). Despite considerable study by both static and dynamic compression methods, many questions still remain unanswered regarding the effect of the degree of nonstoichiometry, the deviatoric stress, and temperatures on the phase boundaries and the equations of state. In order to address these issues, we have conducted a series of static compression experiments on Fe_xO over a wide composition range under hydrostatic and nonhydrostatic conditions.

EXPERIMENTAL PROCEDURE

Sample synthesis and characterization

The physical properties and structural states of Fe_xO are complicated by its nonstoichiometric nature. The syn-

thesized Fe_xO samples often retain a memory of their thermal and pressure history. Careful characterization of the starting materials is very important for interpreting the high-pressure data of Fe_xO. Three synthetic Fe_xO samples ($Fe_{0.92}O$, $Fe_{0.94}O$, and $Fe_{0.98}O$) were used in the experiments. The $Fe_{0.92}O$ and $Fe_{0.94}O$ samples were prepared by heating Fe_2O_3 to 1473 K under controlled oxygen fugacity in a $CO-CO_2$ gas-mixing furnace. The compositions of the samples were determined by x-ray diffraction measurements on the basis of the composition-lattice parameter relationship of Fe_xO (x = [a_0 - 3.900]/0.433, SIMONS, 1980). The lattice parameters of the synthesized samples are $a_0 = 4.296(1)$ Å and $a_0 = 4.307(1)$ Å, corresponding to compositions $Fe_{0.92}O$ and $Fe_{0.94}O$, respectively. The $Fe_{0.98}O$ sample was synthesized from a mixture of $Fe_{0.94}O$ and metallic Fe at 9 GPa and 1273 K in a multi-anvil apparatus. Its lattice parameter is $a_0 = 4.323(1)$ Å.

High-pressure and high-temperature techniques

High pressures were generated between two gem-quality single-crystal diamonds in a diamond-anvil cell, similar to that described by MAO et al. (1979). In order to achieve simultaneous high pressure and temperature, an external resistance heating system was incorporated in the diamond-anvil cell. The cell was accordingly modified to optimize pressure generation at high temperature (MAO et al., 1991). The major modifications include (1) inconel piston-cylinder, (2) thermally insulating the piston-cylinder from the lever arm body, and (3) a double-ring alignment system on the piston to freely retract and advance the piston at high temperature.

Two types of external resistance heating designs were used to achieve high temperature in the diamond-anvil cell in this study. A large sleeve-shaped platinum-wire heater fitted around the protruding portion of the piston-cylinder was used to heat the sample to temperatures up to 900 K (MAO et al., 1991; FEI et al., 1992). This design is not advantageous for generating high pressures >40 GPa) at temperatures above 600 K because of stress relaxation through plastic flow at high temperature. To overcome the problem, we designed a double-heater configuration in which an additional small molybdenum-wire heater was positioned around the diamond anvils (Fig. 1). This double-heater high-temperature diamond-anvil cell is capable of achieving pressures greater than 125 GPa at temperatures up to 1100 K in a mildly reducing atmosphere (Ar with 1% H_2) (FEI and MAO, 1994).

Sample configurations

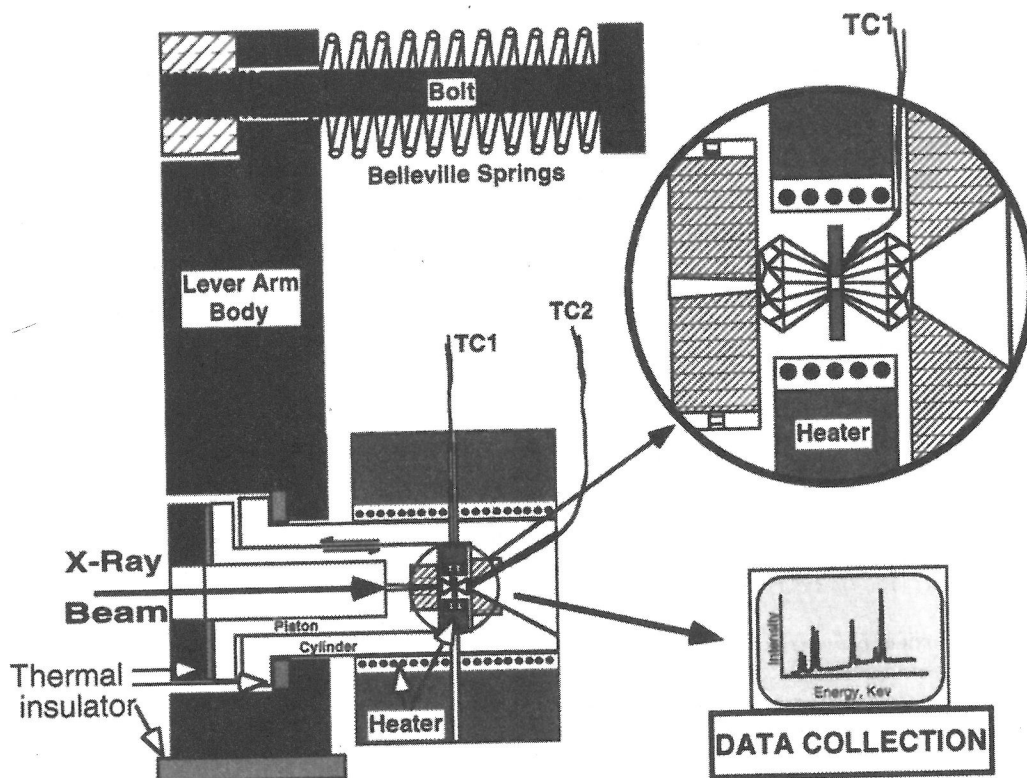Experiments on Fe_xO were conducted under both hydrostatic and nonhydrostatic environments. In the hydro-

FIG. 1. Experimental configuration. The design of the diamond-anvil cell is similar to that of MAO et al. (1991). High temperatures were achieved by using a double-heater system. Temperatures were measured with thermocouples (TC1 and TC2). Energy-dispersive x-ray diffraction techniques were used for data acquisition.

static compression experiments, neon was used as a pressure-transmitting medium. The polycrystalline sample was loaded into a sample chamber, 200 μm in diameter by 70 μm in thickness, drilled from a preindented rhenium gasket. Only one-third of the chamber volume was filled with sample. Small ruby grains and gold foil were placed in the sample chamber as pressure calibrants. The sample chamber was then filled with neon gas at 200 MPa in a high-pressure gas-loading device (JEPHCOAT *et al.*, 1987) and subsequently sealed at pressures above 1 GPa. All the hydrostatic compression experiments were carried out at pressures below 36 GPa, using 600-μm flat diamond anvils. The nonhydrostatic compression experiments were designed to generate higher pressures, using 300-μm culet or beveled diamond anvils. Similar to the hydrostatic compression experiments, the rhenium gasket was preindented to the desired thickness. The powder sample with thin gold foil was compacted in a sample chamber, typically 75 μm in diameter by 25 μm in thickness. The rhenium gasket works very well at high temperature because of its high strength. A simultaneous pressure of 100 GPa and temperature of 1100 K was achieved in this sample configuration.

Synchrotron X-ray diffraction techniques

The experiments were conducted at x17c beamline, the National Synchrotron Light Source, Brookhaven National Laboratory. Polychromatic (white) wiggler synchrotron x-radiation was used for energy-dispersive x-ray diffraction measurements. A highly collimated x-ray beam, regulated by two mutually perpendicular slits, was aligned with the detection system and the center of the sample chamber in the diamond-anvil cell. The sample can be scanned in vertical and horizontal directions by a motor system installed in the sample stage. A 25-μm beam spot was used in diffraction measurements. The diffraction data were collected with an intrinsic germanium 4096-channel solid-state detector at a fixed 2θ angle. The energy-channel number relationship was determined by measuring the energies of well-determined x-ray emission lines (K_α and K_β) of Mn, Cu, Rb, Mo, Ag, Ba, and Tb. The 2θ angle was calibrated by measuring the energies of diffraction peaks, corresponding to the known interplanar spacings d_{hkl}, of gold at ambient conditions.

The energy-dispersive x-ray diffraction technique has the advantage of quick acquisition of diffraction data. Although it is not a problem to maintain simultaneous high pressure and temperature in the high-temperature diamond-anvil cell for extended period of time, quick data acquisition helps to obtain sufficient data over a wide P-T range within the allocated short synchrotron beam time. The diffraction of Fe$_x$O is relatively strong. A complete diffraction pattern of Fe$_x$O with reasonable signal-to-noise ratio can be obtained in less than 10 minutes. The diffraction data were fitted to Voight functions using a peak-fitting program. The interplanar spacings d_{hkl} (Å) were calculated from the measured peak energies E_{hkl} (kev) by $d_{hkl} = (6.199/\sin \theta)/E_{hkl}$.

Temperature and pressure measurements

It is essential to establish a pressure calibration standard at high temperature for the high P-T experiments. At room temperature, pressures in the diamond-anvil cell were determined by measuring the specific volumes of metals such as Cu, Mo, Pd, Ag, Au, and Pt by x-ray diffraction,

based on their volume-pressure relationships derived from shock compression data. The ruby pressure scale was established by measuring simultaneously the shift of the ruby R_1 luminescent line and the specific volume of those metals (MAO *et al.*, 1978; 1986). In this study, pressures at high temperature were determined from the measured lattice parameter of gold and sample temperature, based on the P-V-T equation of state of gold proposed by ANDERSON *et al.* (1989). The sample temperatures were measured with a Pt-Pt13%Rh thermocouple placed near the sample chamber (Figure 1). The temperature difference between the sample and the thermocouple junction is calibrated by observing the melting point of NaCl at ambient pressure. The accuracy and precision of measurements are within 10 K.

RESULTS AND DISCUSSION

Phase relations

The phase transitions in Fe$_x$O were determined by in situ synchrotron x-ray diffraction techniques. In the experiment where Fe$_{0.92}$O powder was used as starting material, we confirmed the transition from the NaCl-type cubic (B1) to a rhombohedral phase at 16 GPa and 300 K under hydrostatic conditions (in a neon pressure transmitting medium). The transition was characterized by the splitting of the 111, 220, and 222 diffraction peaks of the cubic phase (*cf.* Fig. 2). The 200 peak remained sharp and strong. The observed new diffraction pattern
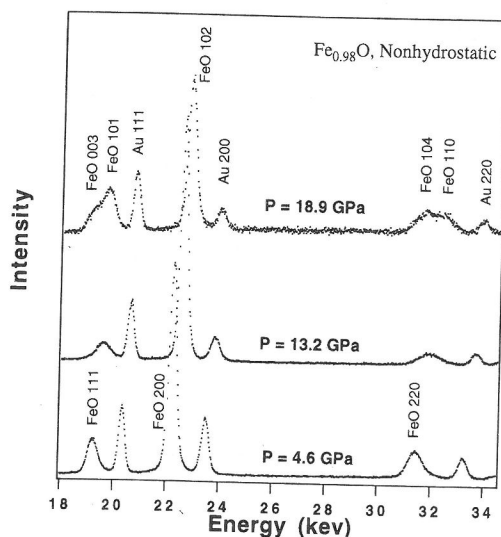

FIG. 2. Energy-dispersive x-ray diffraction spectra of Fe$_x$O at pressures across the cubic-rhombohedral transition under nonhydrostatic conditions. Under hydrostatic conditions, the splitting of the 111 and 220 peaks of the cubic phase occurred in a small pressure interval ($\sim$1 GPa).

can be indexed by using a rhombohedral cell at pressures near the transition, as shown by YAGI et al. (1985). The cubic-rhombohedral transition was also supported by the single-crystal compression experiment where helium was used as pressure medium (MAO et al., 1993). The rhombohedral cell is closely related to the NaCl-type cubic cell and can be derived by stretching along the body diagonal direction 111 of the cubic cell, as suggested by ZOU et al. (1980). However, with increasing pressure, deviation from the rhombohedral cell becomes evident, even when neon was used as pressure transmitting medium.

After observing the rhombohedral phase at room temperature, we started to heat the sample at 22 GPa. The rhombohedral phase transformed back to the cubic phase at 21 GPa and 400 K (Fig. 3). The small pressure drop was due to material relaxation at high temperature. With further increase of pressure at 400 K, the transition from the cubic to the rhombohedral phase was observed again at 23 GPa. Similarly, the transition was observed at 31 GPa and 500 K. At the maximum simultaneous pressure and temperature of 37 GPa and 600 K, the cubic phase was observed. The P-T path of the experiment is shown by the arrows in Fig. 3. The transition boundary has a positive pressure-temperature slope with $P(GPa) = -5.0 + 0.070(\pm0.003)T(K)$.

To evaluate the effect of degree of nonstoichiometry on the transition pressures, we also carried out an experiment where $Fe_{0.98}O$ powder was used as starting material, using neon as pressure transmit-

ting medium. The observed transition pressures at 300 K, 400 K, and 500 K were identical to those of $Fe_{0.92}O$ described above, within experimental uncertainty (±0.4 GPa). The observation at 300 K is also consistent with that of YAGI et al. (1985) who used a $Fe_{0.98}O$ sample in their experiment.

From the experimental results of ZOU et al. (1980) and YAGI et al. (1985), it is evident that the transition from the cubic to the rhombohedral phase is affected by the stress environments of the sample. ZOU et al. reported the transition at 9 GPa and 298 K when no pressure medium was used in the experiment. In contrast to the sharp transition at 16 GPa under hydrostatic conditions (YAGI et al., 1985), the transition pressures cannot be clearly defined under nonhydrostatic conditions. We found that the broadening of the 111 and 220 diffraction peaks occurred at pressures below 8 GPa. The lattice parameters calculated from the 111, 200, and 220 lines indicate significant deviation from the cubic cell at pressures above 6 GPa and room temperature. If we define the transition by the mismatches of the observed and calculated interplanar d_{hkl} spacings, the transition pressure is about 6 GPa at room temperature, 10 GPa lower than that under hydrostatic conditions. The measured pressure-temperature slope (dT/dP) of the transition is lower than the hydrostatic value, resulting from the change of the stress environment with increasing temperature (Fig. 3).

At ambient pressure, Fe_xO undergoes a magnetic transition from paramagnetic to antiferromagnetic state at 198 K (TOMBS and ROOKSBY, 1950; WILLIS and ROOKSBY, 1953; and ROTH, 1960). The magnetic transition was also observed at high pressure and room temperature by high-pressure Mössbauer studies (VAUGHAN and DRICKAMER, 1967; and ZOU et al., 1980). The antiferromagnetic phase has a rhombohedral cell, derived from distortion of the NaCl-type cubic cell, with the rhombohedral angle $a = 59.4°$ at 90 K (WILLIS and ROOKSBY, 1953). ZOU et al. (1980) and YAGI et al. (1985) suggested that the high-pressure transition from the cubic to the rhombohedral phase was the extension of the low-temperature transition caused by the increase of the Néel temperature with pressure. Linear extrapolation of our measured cubic-rhombohedral boundary to ambient pressure yielded the Néel temperatures of 71 K and 250 K for hydrostatic and nonhydrostatic compression, respectively. The discrepancy on the Néel temperature at ambient pressure may result from the complex effect of the stress conditions on the transition. The rhombohedral angle α is about 57.7° ($\pm0.3°$) for the high-pressure rhombohedral phase at 20 GPa and 300
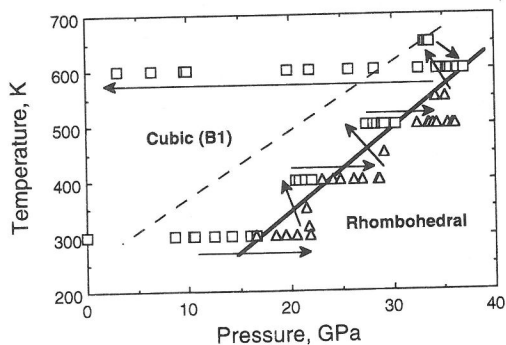

FIG. 3. The cubic-rhombohedral transition determined by in situ x-ray diffraction measurements. The arrows indicate the P-T path of the experiment. The solid and dashed lines represent phase boundaries under hydrostatic and nonhydrostatic conditions, respectively. Experimental data (squares, cubic phase; and triangles, rhombohedral phase) are shown for the $Fe_{0.92}O$ sample. Similar results were obtained when $Fe_{0.98}O$ was used as the starting material.
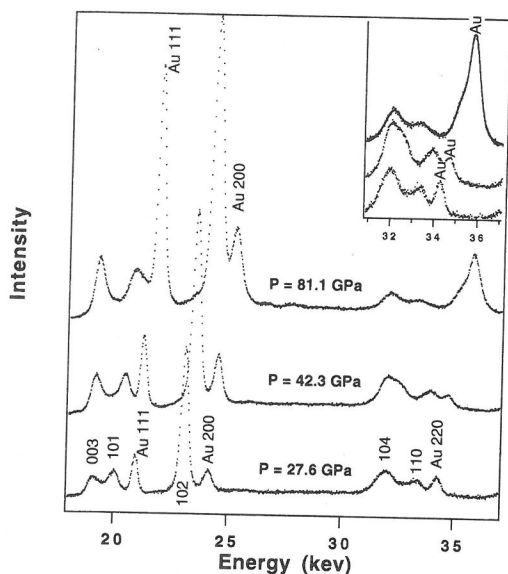
FIG. 4. Energy-dispersive x-ray diffraction spectra of Fe$_x$O at pressures above 27 GPa. At pressures below 40 GPa, the diffraction pattern can be qualitatively indexed with a rhombohedral cell. With increasing pressure, the splitting of the 104 peak was observed, as shown in the inset.

K, which indicates that the degree of distortion at high pressure is higher than that at low temperature.

Although the 111 and 220 peaks begin to broaden at pressures as low as 5 GPa under nonhydrostatic conditions, clear splitting of the 111 and 220 peaks was resolved at pressures above 16 GPa (Fig. 2). The two peaks resulting from the splitting of 111, corresponding to 003 and 101 in the rhombohedral cell assignment, were significantly broader than the 102 peak, corresponding to 200 in the cubic cell. Similarly, the 104 and 110 peaks, of the split 220 in the cubic cell, were very broad. Having examined the diffraction data from three nonhydrostatic compression experiments of Fe$_{0.94}$O and Fe$_{0.98}$O up to 58 GPa, 71 GPa and 82 GPa, respectively, at room temperature, we observed changes in the relative intensities of the 003 and 101 diffractions, indicating strong preferred orientation. Furthermore, the deviation from the rhombohedral cell increases with increasing pressure. At pressures above 40 GPa, further splitting of the 104 peak was observed (Fig. 4), indicating further distortion from the rhombohedral cell to a lower symmetry phase. YAGI et al. (1985) reported evidence of further splitting of the 104 peak at about 40 GPa, but the observed peak was very weak. From our diffraction data, the existence of the

lower symmetry phase is evident, but the nature of this lower symmetry phase is unclear. Our data also indicate that degree of the distortion increases with increasing degree of nonstoichiometry, reflected by the separation of the 003 and 101 peaks in Fe$_{0.94}$O and Fe$_{0.98}$O at any given pressure.

Shock wave studies revealed the existence of a denser phase of Fe$_x$O at pressures above 70 GPa along the Hugoniot (JEANLOZ and AHRENS, 1980; and YAGI et al., 1988). Transition to this denser phase was not observed in static compression experiments at room temperature (YAGI et al., 1985; this study). The structure of this denser phase was the subject of speculation (e.g., JEANLOZ and AHRENS, 1980; JACKSON and RINGWOOD, 1981; NAVROTSKY and DAVIES, 1981; and JACKSON et al., 1990). JACKSON and RINGWOOD (1981) and NAVROTSKY and DAVIES (1981) argued that the denser phase may have the NiAs structure based on thermochemical systematics. Very recently, FEI and MAO (1994) discovered a NiAs-type hexagonal phase of Fe$_x$O at high pressure and temperature by in situ x-ray diffraction measurements. Under nonhydrostatic conditions, the distorted rhombohedral phase transformed to the NiAs phase with transition pressure $P(\text{GPa}) = 118(\pm 2) - 0.051 \times (\pm 0.004)T(\text{K})$ (Fig. 5) (FEI and MAO, 1994). On the basis of this transition and the transition from the cubic to the rhombohedral phase discussed above, the cubic phase (B1) would directly trans-
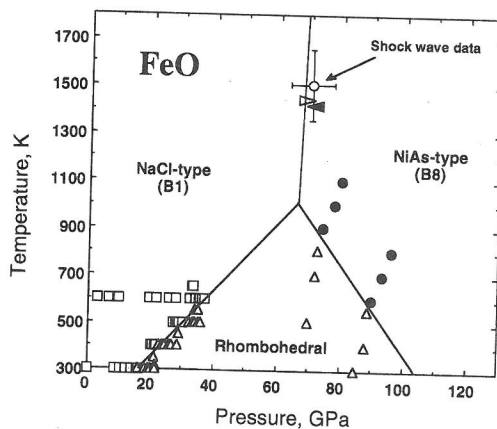

FIG. 5. Phase diagram of Fe$_x$O. Data are shown by symbols: open squares, NaCl structure (B1); open triangles, rhombohedral phase; and solid circles, NiAs-type structure (B8) (FEI and MAO, 1994). Shock-induced transition point (JEANLOZ and AHRENS, 1980) is represented by open circle. The open and solid arrows indicate metallization of FeO inferred from electrical resistance measurements in the laser-heated diamond-anvil cell (KNITTLE and JEANLOZ, 1991).

form to the NiAs phase (B8) at temperatures above the triple point temperature ($\sim$1020 K). The transition from the cubic to the NiAs phase at high pressure and temperature is consistent with the observation of the shock-wave compression experiments.

Isothermal bulk modulus

The compression behavior of Fe_xO has been studied by ultrasonic and shock-wave compression methods and by static compression in the diamond-anvil cell, as reviewed by JEANLOZ and HAZEN (1983) and JACKSON *et al.* (1990). The bulk modulus for the cubic phase (B1) of Fe_xO has a large uncertainty, derived from the static compression data (WILL *et al.*, 1980; HAZEN, 1981; YAGI *et al.*, 1985; JEANLOZ and SATO-SORENSEN, 1986; and LIU and LIU, 1987). The scattering of the compression data, especially at pressures above 6 GPa, is largely due to the deviatoric stress effect under nonhydrostatic environments. We have carried out compression experiments of Fe_xO under hydrostatic and nonhydrostatic conditions and observed similar data scattering when no pressure medium was used in the experiments. Under nonhydrostatic condi-

tions, the diffraction peaks broadened with increasing pressure. The mismatches of d_{111}, d_{200}, and d_{220} were about 0.3 % at 6 GPa, increasing to 1 % at 8 GPa. The lattice parameter of the B1 phase is very sensitive to the deviatoric stress. Even when a soft pressure transmitting medium is used in the experiments, it is important to have sufficiently large medium to sample volume ratio to prevent premature bridging of the diamond anvils by the sample at high pressure. To evaluate the effect of the degree of nonstoichiometry on the bulk modulus, we obtained compression data on $Fe_{0.98}O$ and $Fe_{0.92}O$, using neon as pressure transmitting medium (Table 1, Fig. 6). The volumes were calculated by fitting the d_{111}, d_{200}, and d_{220} spacings, while the pressures were determined using gold as an internal pressure calibrant. In the $Fe_{0.98}O$ experiment, pressures were also determined by using the ruby pressure scale to check the consistency in pressure determination. Least-squares fits of the compression data to the Birch-Murnaghan equation of state yielded the bulk moduli K_{T0} of 147($\pm$2) GPa and 144($\pm$2) GPa for $Fe_{0.92}O$ and $Fe_{0.98}O$, respectively, assuming the pressure derivative $(\partial K_{T0}/\partial P)_T = 4$. The result does not show any significant

Table 1. Hydrostatic compression data of $Fe_{0.92}O$ and $Fe_{0.98}O$ at room temperature

$Fe_{0.92}O$		$Fe_{0.98}O$		
P, GPa[a]	V, cm3/mol	P, GPa[a]	P(ruby), GPa[b]	V, cm3/mol
0.0001	11.93(1)	0.0001	-	12.16(1)
0.81(10)	11.86(1)	1.90(5)	1.80	12.04(1)
1.55(12)	11.79(1)	3.24(6)	-	11.91(1)
2.63(8)	11.73(2)	4.96(16)	5.20	11.76(1)
4.58(15)	11.58(1)	7.61(16)	7.70	11.60(2)
8.65(29)	11.31(1)	8.91(19)	9.00	11.51(1)
10.51(27)	11.20(1)	10.50(10)	10.43	11.40(1)
12.47(30)	11.09(2)	11.49(12)	11.34	11.32(2)
14.19(56)	11.01(2)	12.12(40)	12.34	11.34(2)
16.02(12)	10.90(2)	13.14(31)	13.19	11.27(2)
		13.94(26)	-	11.19(2)
		14.50(30)	14.80	11.17(2)
		15.60(23)	15.90	11.10(2)

[a]Calculated from the lattice parameter of gold, based on its *P-V-T* equation of state proposed by ANDERSON *et al.* (1989). The uncertainties in pressure were propagated from the errors in lattice parameter measurements.

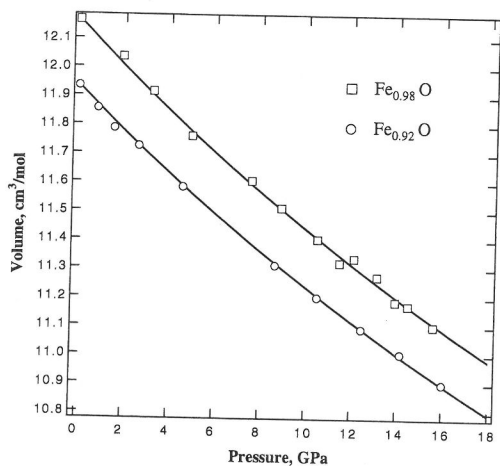[b]Determined by using the ruby pressure scale (MAO *et al.*, 1986)

FIG. 6. Hydrostatic compression data of $Fe_{0.92}O$ (open circles) and $Fe_{0.98}O$ (open squares) at room temperature. The solid curves are calculated isotherms.

effect of the degree of nonstoichiometry on the bulk modulus over the composition range from x = 0.92 to 0.98, contrary to the speculation on the compositional dependence of Fe_xO bulk modulus (MCCAMMON, 1993). A similar conclusion was also reached by HAZEN (1981) who determined the bulk moduli of $Fe_{0.90}O$, $Fe_{0.93}O$, and $Fe_{0.947}O$ using methanol-ethanol (4:1) as pressure medium by the single-crystal diffraction method.

There is some confusion in the comparison of the bulk moduli of Fe_xO derived from static compression data, because the comparisons were made without specifying the pressure derivatives. It is important to evaluate the correlation between the bulk modulus and its pressure derivative, especially when the compression range is limited (JEANLOZ, 1981). To compare the compression data with different compositions, we plotted the relative volume, V/V_0, as a function of pressure. Fig. 7 shows all the hydrostatic or quasi-hydrostatic compression data of the cubic
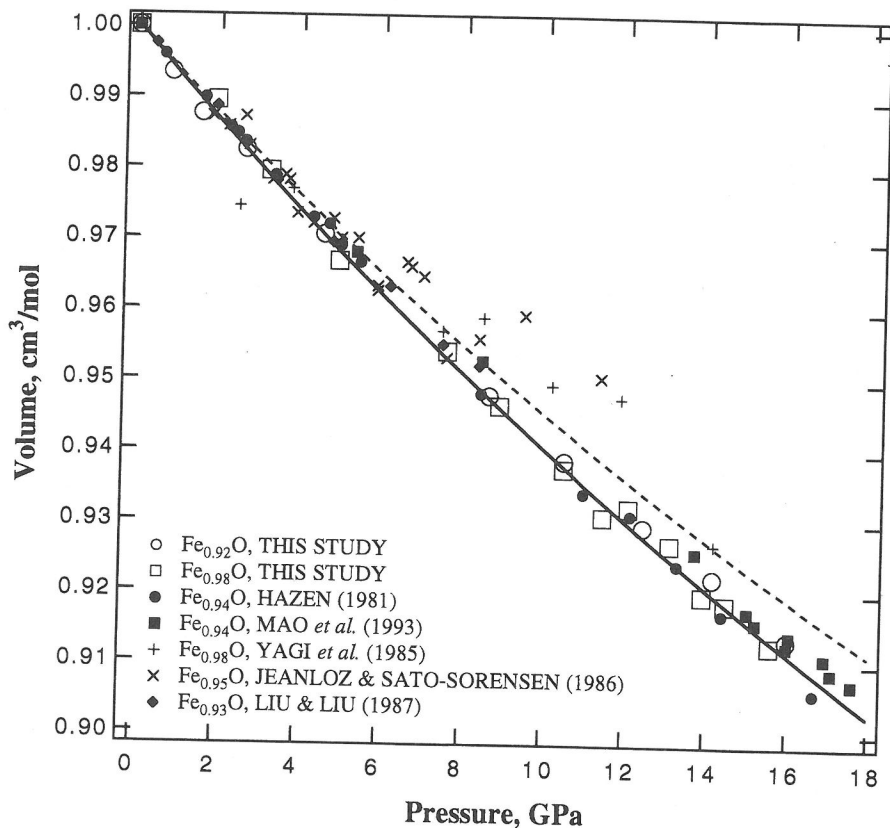

FIG. 7. Comparison of the hydrostatic compression data of Fe_xO. The solid curve is a least-squares fit of all the data except those of YAGI et al. (1985) and JEANLOZ and SATO-SORENSEN (1986) to the Birch-Murnaghan equation of state. The isentrope based on $K_{S0} = 154.9$ GPa and $(\partial K_{S0}/\partial P)_S = 4.84$ derived from the ultrasonic data (JACKSON et al., 1990) are also shown for comparison (the dashed curve).

Y. Fei

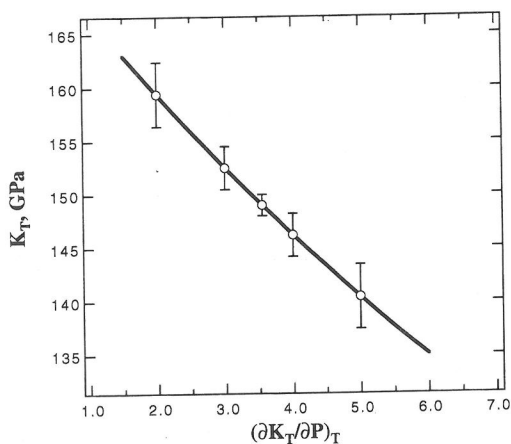

FIG. 8. The trade-off between the bulk modulus K_{T0} and its pressure derivative $(\partial K_{T0}/\partial P)_T$. The best-fit results are K_{T0} = 149 GPa and $(\partial K_{T0}/\partial P)_T$ = 3.5.

Fe_xO phase. The data obtained in this study, using neon as pressure medium, are consistent with the single-crystal studies of HAZEN (1981) who used methanol-ethanol (4:1) as pressure medium and of MAO et al. (1993) who used helium as pressure medium. Our result is also in a good agreement with that of LIU and LIU (1987) who obtained the compression data up to 8.3 GPa using powder x-ray diffraction method. In comparison with the data of YAGI et al. (1985) and JEANLOZ and SATO-SORENSEN (1986) who used methanol-ethanol (4:1) as pressure medium, there is general agreement between our data and their data at pressures below 6 GPa. However, their data at pressures above 6 GPa showed relatively large scatter which may result from the increase of nonhydrostatic stress with increasing pressure.

The Fe_xO samples used to obtain the compression data plotted in Fig. 7 represent a wide range of compositions ($0.90 \leq x \leq 0.98$). There is no systematic effect of the degree of nonstoichiometry on the bulk modulus within the uncertainties of the data. Least-squares fits of all the data except those of YAGI et al. (1985) and JEANLOZ and SATO-SORENSEN (1986) to the Birch-Murnaghan equation of state yielded the best-fit results, K_{T0} = 149 GPa and $(\partial K_{T0}/\partial P)_T$ = 3.5. However, The K_{T0} and $(\partial K_{T0}/\partial P)_T$ are strongly correlated. Figure 8 shows the covariance between K_{T0} and $(\partial K_{T0}/\partial P)_T$.

JEANLOZ and HAZEN (1983) pointed out that the bulk moduli determined by dynamic methods, including ultrasonic and shock-wave experiments, were significantly higher than those obtained by static compression. Recent ultrasonic measurements indicate

that the bulk moduli of single-crystal Fe_xO determined by ultrasonic wave propagation have very small variation, ranging from 151 GPa to 154 GPa (BERGER et al., 1981; and JACKSON et al., 1990). The bulk moduli determined by resonance techniques (SUMINO et al., 1980), by polycrystalline ultrasonic measurements (MIZUTANI, 1971; and BONCZAR and GRAHAM, 1982), and by shock-wave compression (JEANLOZ and AHRENS, 1980) range from 172 GPa to 182 GPa. JACKSON et al. (1990) showed that essentially all of the previous ultrasonic, static and shock compression data could be reconciled with their K_{S0} and $(\partial K_{S0}/\partial P)_S$ values of 155 GPa and 4.9 respectively. However, assessment of the hydrostatic compression data of Fe_xO (HAZEN, 1981; MAO et al., 1993; this study) shows a lower bulk modulus, K_{T0} = 149 GPa, for a $(\partial K_{T0}/\partial P)_T$ value of 3.5. The ultrasonic and static compression data could be reconciled with the ultrasonic value (K_{T0} = 153 GPa), if a $(\partial K_{T0}/\partial P)_T$ value of 3.1 is assumed.

The bulk modulus for the rhombohedral phase of Fe_xO was not well constrained because the powder diffraction data for the rhombohedral phase were limited between 16 GPa and 23 GPa. The data collected above 23 GPa under nonhydrostatic conditions indicated significant deviation from the rhombohedral cell, and also indicated further distortion to a lower symmetry phase. Despite the splitting and broadening of the 111, 220, and 311 peaks, the 200 of the cubic phase, corresponding to the 102 in the rhombohedral cell, remained sharp and strong. The pressure dependence of the d spacing of this peak (Fig. 9) indicates that the rhombo-
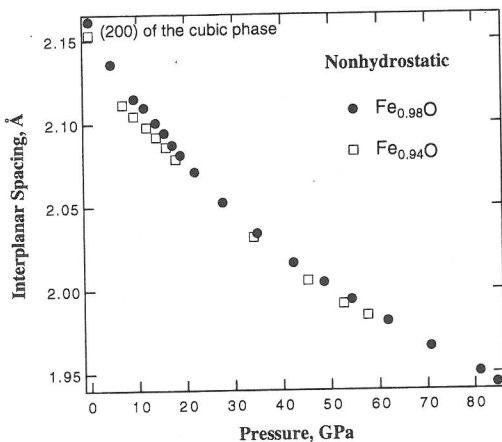

FIG. 9. Pressure dependence of the interplanar d spacings related to the 200 peak of the cubic cell. Experimental data are shown for two compositions, $Fe_{0.98}O$ (solid circles) and $Fe_{0.94}O$ (open squares).

hedral phase (or the distorted rhombohedral phase) is less compressible than the cubic phase. The density of the rhombohedral phase is only slightly larger than that of the cubic phase at the transition pressure. The difference in density is about 0.5%.

FEI and MAO (1994) reported the bulk modulus $K_T = 172(\pm14)$ GPa and its pressure derivative $(\partial K_T/\partial P)_T = 4.3(\pm0.6)$ for the NiAs hexagonal phase of Fe_xO at 900 K. Their results are in good agreement with the shock compression data (JEAN-LOZ and AHRENS, 1980; and YAGI et al., 1988). A comparison of the densities of the NiAs hexagonal phase between the static and shock-wave data was shown by FEI and MAO (1994).

It is very difficult to determine the temperature effect on the bulk modulus even for the cubic phase of Fe_xO because the composition of Fe_xO changes as a function of temperature and pressure. Figure 10 shows the results from two high P-T experi-

ments in which neon was used as pressure medium. In the first experiment, a $Fe_{0.92}O$ sample was used as the starting material. Its room temperature compression data were discussed above. Upon heating, the cubic phase is stable to higher pressure (cf. Fig. 3). The lattice parameters for the cubic phase at 400 K and 500 K plotted on the extrapolation of the 300-K compression curve indicate very small thermal expansivity at high pressure (Fig. 10). With further increasing temperature to 600 K, the lattice parameters increased substantially. The change cannot be simply attributed to thermal expansion. After we conducted the experiment with the sample close to the stoichiometric composition, we realized that the sudden change in lattice parameter at 600 K was due to the compositional change. Figure 10 also shows the lattice parameters as a function of pressure from the experiment where $Fe_{0.98}O$ sample was used as the starting material. The lattice
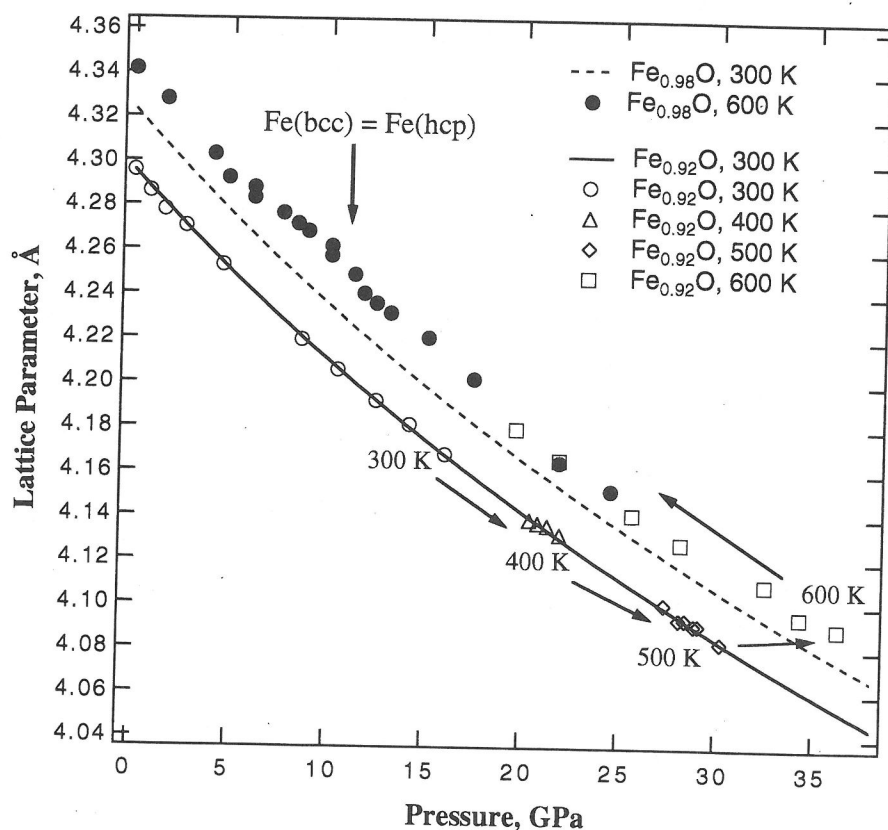

FIG. 10. Lattice parameters of the cubic phase as a function of pressure and temperature. The open symbols are data from the experiment where $Fe_{0.92}O$ was used as the starting material. The solid circles represent compression data of $Fe_{0.98}O$ at 600 K. The solid and dashed curves are the calculated 300-K isotherms of $Fe_{0.92}O$ and $Fe_{0.98}O$, respectively. The arrows indicate the P-T path of the experiment.

parameters at 600 K are consistent with those from the first experiment where the $Fe_{0.92}O$ sample was used as starting material, implying that the Fe_xO samples may have similar equilibrium composition at high pressure and temperature regardless of the compositional differences in the starting materials. Upon decompression at 600 K, a small kink in the lattice parameter was observed at about 11 GPa, coincident with the $\alpha - \epsilon$ transition in Fe. The kink is reproducible upon compression or decompression. If this kink in the lattice parameter reflects the compositional change of Fe_xO, it may explain why the Fe_xO sample with maximum Fe content (close to the stoichiometric composition) can be synthesized at about 10 GPa.

Crystal chemistry

HAZEN and JEANLOZ (1984) reviewed the crystal chemistry and defect structure of Fe_xO at ambient pressure. Our *in situ* x-ray diffraction measurements of Fe_xO provide new data for understanding the crystal chemistry and phase relations of Fe_xO at high pressure and temperature. On the basis of the x-ray diffraction studies (ZOU *et al.*, 1980; YAGI *et al.*, 1985; MAO *et al.*, 1993; and this study), it is quite clear that the 16-GPa transition at room temperature is a cubic to rhombohedral transition caused by distortion of the cubic cell, an elongation along a body diagonal direction (111) of the NaCl-type cubic cell. Our determination of the temperature and stress dependence of the transition supports that this transition is closely related to the observed paramagnetic to antiferromagnetic transition at low temperature, but the degree of the distortion may be a complex function of pressure and stress. The rhombohedral distortion is very sensitive to the sample stress environments. Further distortion to a low symmetry phase at room temperature is evident, but it is not clear if this low symmetry phase is metastable.

At high pressure and temperature, Fe_xO has the NiAs-type hexagonal structure (B8) (FEI and MAO, 1994). The NiAs structure consists of hexagonally close-packed layers of oxygen and iron alternately stacked along the c axis. It can be derived from the NaCl-type cubic cell by varying the stacking along the body diagonal direction (111) of the cubic cell, corresponding to the c axis in the NiAs structure. The Fe-Fe distance in the NiAs structure is about 8% shorter than that in the NaCl structure. The shorter Fe-Fe distance across shared FeO_6 octahedral faces in the NiAs structure could lead to metallization of Fe_xO (JACKSON *et al.*, 1990), supporting the metallic behavior of this phase observed

by electrical resistivity measurements (KNITTLE and JEANLOZ, 1986, 1991; and KNITTLE *et al.*, 1986). The increase of metallicity of Fe_xO at high pressure would enhance oxygen solubility (in the form of FeO) in molten iron, which has important implications for the incorporation of lighter elements into the Earth's core (FEI and MAO, 1994).

It is well documented that Fe_xO exsolves iron or magnetite lamellae on the scale of several tens of unit cells (HAZEN and JEANLOZ, 1984). The exsolution in Fe_xO is the result of equilibrium processes in the system Fe-O. Attempts to model the Fe-Fe_xO equilibria at high pressure and temperature were made previously by MAO, 1974; FEI and SAXENA, 1986; and McCAMMON, 1993. Those models were based on the results from quenched experiments. Many measurements and observations were difficult to interpret as a result of complexities in quenching thermal and pressure history. In this study, we provided new *in situ* measurements on lattice parameters of Fe_xO as a function of pressure and temperature (Fig. 10). To completely understand equilibrium processes in the Fe-Fe_xO system at high pressure and temperature, more *in situ* measurements in pressure-temperature-composition space are required.

CONCLUSIONS

Despite the complexities in physical properties and structure states of Fe_xO at high pressure and temperature, a clear picture of its phase relations and compression behavior is begining to emerge. On the basis of our experimental results, we can conclude that the cubic-rhombohedral phase transition boundary is not affected by the degree of nonstoichiometry of Fe_xO, but is strongly dependent on the deviatoric stress environment. The bulk modulus for the cubic phase, derived from hydrostatic compression data, is $K_{T0} = 146$ GPa with its pressure derivative $(\partial K_{T0}/\partial P)_T = 4$, independent of the degree of nonstoichiometry of Fe_xO. Under nonhydrostatic conditions, the rhombohedral phase increases its distortion with increasing pressure. A lower symmetry phase, resulting from the rhombohedral distortion, was observed at pressures above 40 GPa and room temperature. The structure and nature of this lower symmetry phase are still not clear. Transition from the rhombohedral distortion to a NiAs-type hexagonal phase was observed upon heating, consistent with shock compression experiments. The transition has been studied only for composition $Fe_{0.98}O$. Therefore, the effect of the degree of nonstoichiometry still needs to be addressed.

The effect of Mg content on the transitions observed in Fe_xO has important implications for lower mantle mineralogy. We carried out one experiment on $(Fe_{0.95}, Mg_{0.05})O$. The transition from the cubic to rhombohedral phase was observed. However, no NiAs-type hexagonal phase was observed up to 101 GPa and 600 K. Evidently, further study is required to understand the role of Mg in the transitions at high pressure and temperature.

REFERENCES

ANDERSON O. L., ISAAK D. G. and YAMAMOTO S. (1989) Anharmonicity and the equation of state for gold. *J. Appl. Phys.* **65**, 1534–1543.

BERGER J., BERTHON J., REVCOLEVSCHI A. and JOLLES E. (1981) Elastic constants of $Fe_{1-x}O$ single crystals. *J. Am. Ceram. Soc.* **64**, C153–C154.

BONCZAR L. J. and GRAHAM E. K. (1982) The pressure and temperature dependence of the elastic properties of polycrystal magnesiowüstite. *J. Geophys. Res.* **87**, 1061–1078.

FEI Y. and MAO H. K. (1991) In-situ x-ray diffraction study of wüstite ($Fe_{0.947}O$) up to 70 GPa and 600 K (abstr.). *EOS* **72**, 465.

FEI Y. and MAO H. K. (1994) In-situ determination of the NiAs phase of FeO at high pressure and temperature. *Science* **266**, 1678–1680.

FEI Y. and SAXENA S. K. (1986) A thermochemical data base for phase equilibria in the system Fe-Mg-Si-O at high pressure and temperature. *Phys. Chem. Mineral.* **13**, 311–324.

FEI Y., MAO H. K., SHU J. and HU J. (1992) *P-V-T* equation of state of magnesiowüstite ($Mg_{0.6}Fe_{0.4}$)O. *Phys. Chem. Miner.* **18**, 416–422.

HAZEN R. M. (1981) Systematic variation of bulk modulus of wüstite with stoichiometry. *Year Book Carnegie Inst. Washington* **80**, 277–280.

HAZEN R. M. and JEANLOZ R. (1984) Wüstite ($Fe_{1-x}O$): A review of its defect structure and physical properties. *Rev. Geophys. Space Phys.* **22**, 37–46.

ITO E., MOROOKA K., UJIKE O. and KATSURA T. (1995) Reactions between molten iron and silicate melts at high pressure: Implications for the chemical evolution of the Earth's core. *J. Geophys. Res.* **100**, 5901–5910.

JACKSON I. and RINGWOOD A. E. (1981) High-pressure polymorphism of the iron oxides. *Geophys. J. R. Astron. Soc.* **64**, 767–783.

JACKSON I., KHANNA S. K., REVCOLEVSCHI A. and BERTHON J. (1990) Elasticity, shear-mode softening and high-pressure polymorphism of wüstite ($Fe_{1-x}O$). *J. Geophys. Res.* **95**, 21,671–21,685.

JEANLOZ R. (1981) Finite-strain equation of state for high-pressure phases. *Geophys. Res. Lett.* **8**, 1219–1222.

JEANLOZ R. and AHRENS T. J. (1980) Equations of state of FeO and CaO. *Geophys. J. R. Astron. Soc.* **62**, 505–528.

JEANLOZ R. and HAZEN R. M. (1983) Compression, non-stoichiometry and bulk viscosity of wüstite. *Nature* **304**, 620–622.

JEANLOZ R. and SATO-SORENSEN Y. (1986) Hydrostatic compression of $Fe_{1-x}O$ wüstite. *J. Geophys. Res.* **91**, 4665–4672.

JEPHCOAT A. P., MAO H. K. and BELL P. M. (1987) Operation of the megabar diamond-anvil cell. In *Hydrothermal Experimental Techniques* (ed. G. C. ULMER and H. L. BARNES), pp. 469–506. Wiley-Interscience, New York.

KATO T. and RINGWOOD A. E. (1989) Melting relationships in the system Fe-FeO at high pressure: Implications for the composition and formation of the Earth's core. *Phys. Chem. Miner.* **16**, 524–538.

KNITTLE E. and JEANLOZ R. (1986) High-pressure metallization of FeO and implications for the Earth's core. *Geophys. Res. Lett.* **13**, 1541–1544.

KNITTLE E. and JEANLOZ R. (1991) The high-pressure phase diagram of $Fe_{0.94}O$: A possible constituent of the Earth's core. *J. Geophys. Res.* **96**, 16,169–16,180.

KNITTLE E., JEANLOZ R., MITCHELL A. C. and NELLIS W. J. (1986) Metallization of $Fe_{0.94}O$ at elevated pressures and temperatures observed by shock-wave electrical resistivity measurements. *Solid State Commun.* **59**, 513–515.

LIU M. and LIU L. (1987) Bulk moduli of wüstite and periclase: a comparative study. *Phys. Earth Planet. Inter.* **45**, 273–279.

MAO H. K. (1974) A discussion of the iron oxides at high pressure with implications for the chemical and thermal evolution of the Earth. *Year Book Carnegie Inst. Washington* **73**, 510–518.

MAO H. K., TAKAHASHI T., BASSETT W. A., WEAVER J. S. and AKIMOTO S. (1969) Effect of pressure and temperature on the molar volumes of wüstite and of three (Fe, Mg)$_2$SiO$_4$ spinel solid solutions. *J. Geophys. Res.* **74**, 1061–1069.

MAO H. K., BELL P. M., SHANER J. W. and STEINBERG D. J. (1978) Specific volume measurements of Cu, Mo, Pd, and Ag and calibration of the ruby R1 fluorescence pressure gauge from 0.06 to 1 Mbar. *J. Appl. Phys.* **49**, 3276–3283.

MAO H. K., BELL P. M., DUNN K. J., CHRENKO R. M. and DEVRIES R. C. (1979) Absolute pressure measurements and analysis of diamonds subjected to maximum static pressures of 1.3–1.7 Mbar. *Rev. Sci. Instrum.* **50**, 1002–1009.

MAO H. K., XU J. and BELL P. M. (1986) Calibration of the ruby pressure gauge to 800 kbar under quasihydrostatic conditions *J. Geophys. Res.* **91**, 4673–4676.

MAO H. K., HEMLEY R. J., FEI Y., SHU J. F., CHEN L. C., JEPHCOAT A. P., WU Y. and BASSETT W. A. (1991) Effect of pressure, temperature, and composition on lattice parameters and density of (Fe,Mg)SiO$_3$-perovskites to 30 GPa, *J. Geophys. Res.* **96**, 8069–8079.

MAO H. K., SHU J., FEI Y., HU J. and HEMLEY R. J. (1993) High pressure phase transition in $Fe_{1-x}O$ wüstite (abstr.). *EOS* **74**, 169.

McCAMMON C. (1993) Effect of pressure on the composition of the lower mantle end member Fe_xO. *Science* **259**, 66–68.

MIZUTANI H. (1971) Elasticity of mantle minerals and composition of the upper mantle. Ph.D. dissertation, Univ. Tokyo.

NAVROTSKY A. and DAVIES P. K. (1981) Cesium chloride versus nickel arsenide as possible structures for (Mg,

Fe)O in the lower mantle. *J. Geophys. Res.* **86**, 3689–3694.

OHTANI E. and RINGWOOD A. E. (1984) Composition of the core, I. Solubility of oxygen in molten iron at high temperatures. *Earth Planet. Sci. Lett.* **71**, 85–93.

OHTANI E., RINGWOOD A. E. and HIBBERSON W. (1984) Composition of the core, II. Effect of high pressure on solubility of FeO in molten iron. *Earth Planet. Sci. Lett.* **71**, 94–103.

RINGWOOD A. E. (1977) Composition of the core and implications for origin of the earth. *Geochem. J.* **11**, 111–135.

RINGWOOD A. E. and HIBBERSON W. (1990) The system Fe-FeO revised. *Phys. Chem. Miner.* **17**, 313–319.

RINGWOOD A. E. and HIBBERSON W. (1991) Solubilities of mantle oxides in molten iron at high pressures and temperatures: Implications for the composition and formation of Earth's core. *Earth Planet. Sci. Lett.* **102**, 235–251.

ROTH W. L. (1960) Defects in the crystal and magnetic structures of ferrous oxide. *Acta Cryst.* **13**, 140–149.

SIMONS B. (1980) Composition-lattice parameter relationship of magnesiowüstite solid solution series. *Year Book Carnegie Inst. Washington* **79**, 376–380.

SUMINO Y., KUMAZAWA M., NISHIZAWA O. and PLUSCH-KELL W. (1980) The elastic constants of single crystal $Fe_{1-x}O$, MnO and CoO, and the elasticity of stoichiometric magnesiowüstite. *J. Phys. Earth* **28**, 475–495.

TOMBS N. C. and ROOKSBY H. P. (1950) Structure of monoxides of some transition elements at low temperatures. *Nature* **165**, 442–443.

VAUGHAN R. W. and DRICKAMER H. G. (1967) High-pressure Mössbauer studies on a-Fe_2O_3, $FeTiO_3$, and FeO. *J. Chem. Phys.* **47**, 1530–1536.

WILL G., HINZE E. and NUDING W. (1980) The compressibility of FeO measured by energy dispersive x-ray diffraction in a diamond anvil squeezer up to 200 kbar. *Phys. Chem. Miner.* **6**, 157–167.

WILLIS B. T. M. and ROOKSBY H. P. (1953) Change of structure of ferrous oxide at low temperature. *Acta Cryst.* **6**, 827–831.

YAGI T., SUZUKI T. and AKIMOTO S. (1985) Static compression of wüstite ($Fe_{0.98}O$) to 120 GPa. *J. Geophys. Res.* **90**, 8784–8788.

YAGI T., FUKUOKA K., TAKEI H. and SYONO Y. (1988) Shock compression of wüstite. *Geophys. Res. Lett.* **15**, 816–819.

ZOU G., MAO H. K., BELL P. M. and VIRGO D. (1980) High pressure experiments on the iron oxide wüstite ($Fe_{1-x}O$). *Year Book Carnegie Inst. Washington* **79**, 374–376.